

Large Teleseismic P Wavefront Deflections Observed with Broadband Arrays

by Vera Schulte-Pelkum,* Frank L. Vernon, and Jennifer Eakins

Abstract We measure the plane wavefront incidence azimuth for teleseismic P at large-aperture (~ 50 km) broadband arrays. The incidence azimuth is determined by crosscorrelation of the P arrivals on the vertical component seismograms filtered in successive frequency bands. The periods considered range from 10 to 35 sec. At the Anza array in southern California, the plane wave direction is deflected from the great circle azimuth of the event by up to 20° . In addition, we find a surprisingly strong frequency dependence of the same magnitude and a striking antisymmetric pattern of the deflection as a function of backazimuth, whereas the curvature of the wavefront is small. Similar characteristics are found at the Gräfenberg array in Germany and the NORSAR array in Norway, however, with much weaker amplitudes of $\sim 5^\circ$. We ascribe the behavior at Anza to structure in the lower crust and uppermost mantle beneath the array, given that the observations are only a function of source backazimuth and not of source depth and source mechanism, that the wavelengths under consideration range from 50 to 270 km, and that the sign of the deviation is opposite to that predicted from shallow crustal structure and Moho topography. We are able to reproduce the magnitude and frequency dependence of the wavefront deflection using finite difference numerical modeling of plane wave propagation through simple 2D structures.

Introduction

Slowness and azimuthal anomalies of teleseismic P phases measured at seismic arrays have been used to infer mantle and crustal structure. An early controversy was related to whether the anomalies were caused by near-receiver structure in the upper mantle and crust, or in the lower mantle; results are summarized in more recent studies such as Steck and Prothero (1993), Lin and Roecker (1996), and Tibuleac and Herrin (1999). Most of these studies were conducted in the short-period (~ 1 Hz) band. In addition, most recent applications of azimuth determination of seismic phases using arrays are related to location, detection, and discrimination problems, and are therefore more concerned with robustness in the presence of noise and multiple signals (e.g., Harris [1990], Chiou and Bolt [1993], Wagner and Owens [1996]). Once empirical corrections for systematic anomalies or so-called statics are found, they are used to calibrate individual records from the array, but for the most part, the underlying cause is left uninvestigated. In this study, we use very high signal-to-noise teleseismic P arrivals at several broadband, large-aperture arrays to study earth

structure. One novel aspect is the resolution of frequency dependence of azimuthal anomalies within the long-period ($T > 10$ sec) band.

Data

The main focus of this study is the Anza array in southern California. In the configuration used in this study (Fig. 1), the array has nine three-component stations with Streckeisen STS-2 broadband sensors distributed irregularly over an aperture of ~ 50 km. For part of the time under consideration in this study, four additional stations were in operation. All sensors are located on bedrock of the Peninsular Ranges batholith. Despite the large variation in topography over the area, the altitude of the stations used here varies by only ~ 100 m. The array is bisected by the San Jacinto fault, a major branch of the San Andreas fault system.

For comparison with the results from Anza, we also analyzed data from the Gräfenberg broadband array (GRF) (Fig. 2) in southeast Germany. The array consists of 13 stations with STS-1 sensors over an aperture of roughly 50 by 100 km and is located on Jurassic limestone in an area with only slight tectonic activity. A third dataset comes from the NORSAR array (Fig. 3) in southern Norway, with six broad-

*Present address: CIRES and Dept. Geological Sciences, University of Colorado at Boulder, UCB 399, Boulder, Colorado, 80309-0399, vera_sp@cires.colorado.edu.

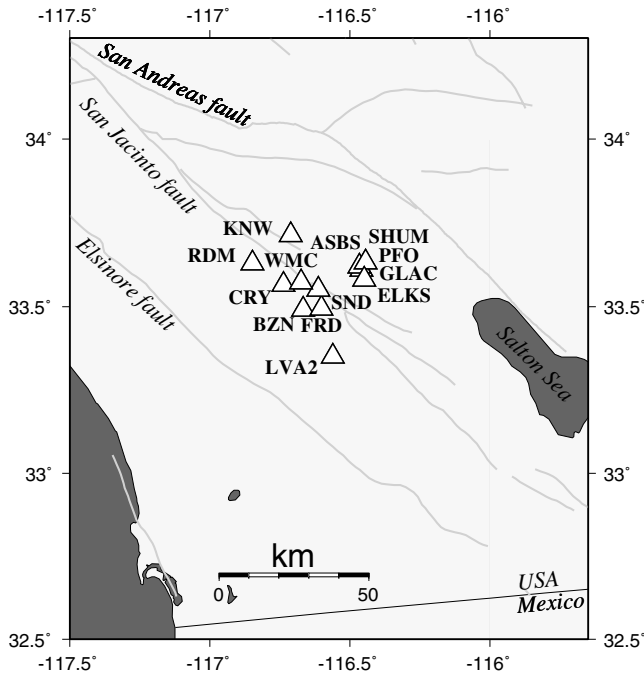


Figure 1. Map of the Anza stations used in this study.

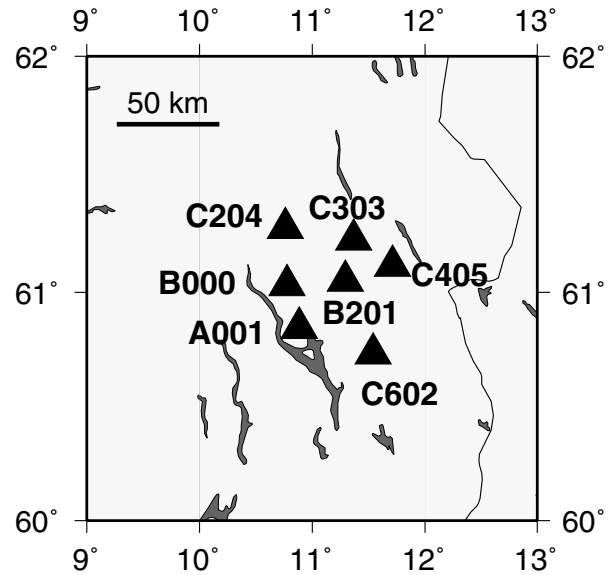


Figure 3. Locations of the three-component broadband stations of the NORSAR array.

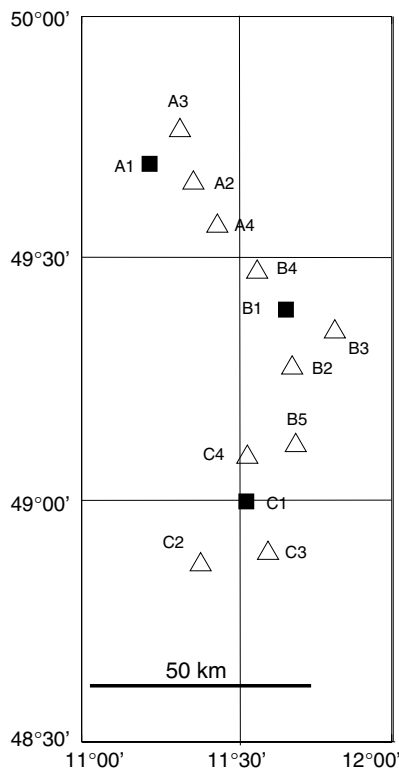


Figure 2. Map of the GRF array. Solid squares mark stations where three-component particle-motion analysis was performed.

band three-component sensors and an aperture of ~ 50 km, located on the Scandinavian shield.

The events analyzed were selected for their extremely high signal-to-noise ratio (pre-event noise amplitude typically $< 1/50$ P amplitude) of the teleseismic P onset in the long-period band (Fig. 4). Body wave magnitudes of the events used range from $m_b = 4.8$ – 6.1 . Event locations and origin times are given in Table 1.

Method

Our interest in this study is in the azimuth of the plane-wave component of the P -wave arrival. To determine the plane-wave azimuth, we calculate relative delays between the P arrivals on the vertical components between all pairs of stations by crosscorrelation, and fit a plane wave to the relative delays using least-squares analysis. An error is estimated by propagating the residuals remaining after the plane wave fit through the solution. Note that we only measure the azimuth of the arrival this way, whereas the incidence angle off the vertical remains undetermined and no assumptions are made regarding the subsurface velocities. The crosscorrelation analysis is performed on the long-period band P onset (10–100 sec period) and also on each event filtered (butterworth) in successive narrow frequency bands with center frequencies of 0.03–0.1 Hz (33–10 sec period) in intervals of 0.01 Hz and bandwidths of 0.02 Hz. Although this narrowband filtering leads to very ringy seismograms, cycle skipping does not occur. Relative delays can be determined to the accuracy allowed by the sample rate of 40 Hz because the array apertures are smaller than the wavelengths in the frequency band under consideration; therefore, the relative time delays determined by crosscorrelation are small compared with the long-period P cycle length. The

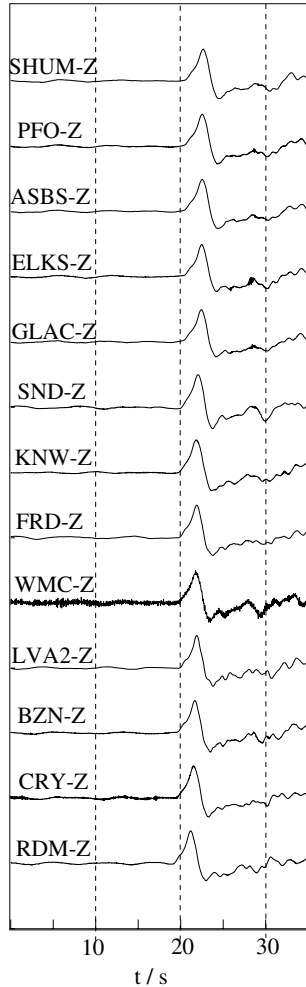


Figure 4. Example of the kind of coherent, high signal-to-noise broadband P onset used in this study. The section shows unfiltered, normalized velocity seismograms on all Anza vertical components, sorted by epicentral distance. See second Anza event in Table 1 for event information.

time windows used for crosscorrelation are one period before to one period after the P arrival predicted by the International Association of Seismology and Physics of the Earth's Interior (IASPEI) earth model (i.e., we use longer time windows at lower frequencies).

We also compare the phase velocity azimuth determined in this fashion with the azimuth of initial P -particle motion measured on the three components of a single station. The multitaper frequency domain method used for the particle motion measurement is described in Schulte-Pelkum *et al.* (2001). We were unable to perform accurate particle-motion measurements on the Anza STS-2 data because of noise on the horizontal components in the long-period band, and therefore used data from the STS-1 sensor at the colocated IDA station PFO (Piñon Flat).

The azimuthal anomalies for both wavefront directions and particle-motion direction are determined relative to the

event location backazimuth based on the National Earthquake Information Center (NEIC) catalog. The sign convention chosen here is a positive azimuthal anomaly for a clockwise deviation of the measured backazimuth relative to the event azimuth.

Results

Figure 5 shows the azimuthal deviation of the slowness direction determined from relative time delays on the Anza vertical components as a function of backazimuth. There is a strong ($\sim 10^\circ$) clockwise deviation for southeastern events and a trend toward smaller anticlockwise deviations for events from the northwest. The same figure shows azimuthal particle-motion deviations measured at PFO close to the center of the Anza array. The deviations for events from the west and northwest agree with the wavefront directions, whereas the sign of the anomaly for events from the southeast is opposite. Unlike the wavefront directions, the particle-motion anomaly shows a distinct π -periodic pattern over backazimuth that we ascribed to azimuthal anisotropy in Schulte-Pelkum *et al.* (2001). The existence of anisotropy explains the discrepancy between particle motion and wavefront direction in general (Crampin *et al.*, 1982). However, the model suggested in Schulte-Pelkum *et al.* (2001) to explain the pattern at PFO (azimuthal anisotropy with a horizontal or dipping symmetry axis in horizontal layers) is insufficient to create a pattern of wavefront deviations as observed here, because horizontal layers do not cause wavefront deviations in azimuth, regardless of azimuthal or any other type of anisotropy.

Even more interesting behavior is seen in the narrow-band wavefront directions. The trend of the azimuthal deviation with backazimuth changes systematically with frequency. Unfortunately, a corresponding analysis of particle-motion direction is hampered by the fact that the frequency resolution of the multitaper method can not achieve comparable detail. There is a strong and systematic frequency dependence of the azimuthal slowness perturbation for each event (Fig. 6). The frequency pattern slowly changes character with changing event backazimuth. The patterns are also highly reproducible between events at similar backazimuths, but they are independent of source depth and therefore presumably not influenced by the near-source path and source mechanism.

A comparison between the anomaly pattern of events on exactly opposite backazimuths shows a very striking antisymmetric behavior (Fig. 7). Flipping the sign of the pattern of one event reproduces very closely the pattern from the opposite event.

For comparison with the Anza results, we performed the same analysis at the NORSAR and GRF arrays. In the case of NORSAR, azimuthal deviations of both the particle motions and the slowness vector are small and consistently positive (i.e., rotated clockwise relative to the backazimuth) for eastern events, and negative for western ones. In addi-

Table 1
Events Used in This Study

Latitude (°)	Longitude (°)	Depth (km)	Date (mm/dd/yyyy)	Day	Time (UTC)*	m_b
<i>Anza</i>						
11.13	-61.00	0	4/22/1997	(112)	9:31:23.6	5.5
-20.41	169.34	69	5/21/1997	(141)	14:10:29.1	5.5
-32.09	179.83	283	5/25/1997	(145)	23:22:29.4	5.4
-35.92	-102.55	0	5/29/1997	(149)	17:02:38.1	5.3
51.27	-179.21	0	6/17/1997	(168)	21:03:36.2	6.1
43.30	146.32	0	7/14/1997	(195)	16:09:31.6	5.4
-29.37	-71.67	0	7/19/1997	(200)	12:22:54.2	5.6
52.60	-167.57	0	7/20/1997	(201)	0:30:19.5	5.1
3.80	-75.59	202	9/02/1997	(245)	12:13:24.3	5.8
-4.29	-76.57	135	10/28/1997	(301)	6:15:22.1	5.8
-19.45	169.32	149	6/29/1995	(180)	12:24:05.6	5.8
5.10	-75.59	131	8/19/1995	(231)	21:43:34.5	5.6
18.90	145.07	603	8/23/1995	(235)	7:06:05.2	5.9
<i>NORSAR</i>						
36.41	70.97	203	5/13/1997	(133)	14:13:47.8	5.8
51.27	-179.21	0	6/17/1997	(168)	21:03:36.2	6.1
38.28	-26.73	17	6/27/1997	(178)	4:39:55.1	4.8
10.49	-63.50	0	7/09/1997	(190)	19:24:10.3	5.3
52.60	-167.57	0	7/20/1997	(201)	0:30:19.5	5.1
30.10	57.50	0	3/14/1998	(073)	19:40:28.0	5.3
53.00	159.99	0	6/01/1998	(152)	5:33:59.3	5.8
-0.48	-80.23	0	8/04/1998	(216)	18:59:16.8	5.6
5.39	126.88	36	9/02/1998	(245)	8:37:31.0	6.1
<i>GRF</i>						
16.80	-93.33	186	10/21/1995	(294)	2:39:00.1	5.6
36.41	70.97	203	5/23/1997	(133)	14:13:47.8	5.8
3.80	-75.59	202	9/02/1997	(245)	12:13:24.3	5.8

*UTC, coordinated universal time.

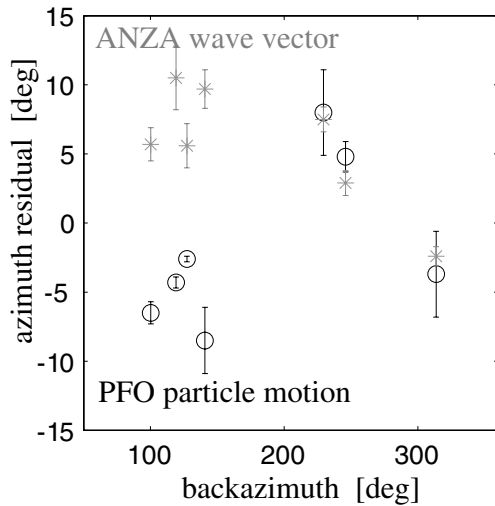


Figure 5. Azimuthal deviation of the slowness vector (grey stars) and the particle motion (circles) from the event location backazimuth at Anza, for the same events. Positive deviations are clockwise.

tion, the magnitude of the anomalies is much smaller (to $\sim 5^\circ$ rather than $\sim 20^\circ$) and the frequency dependence not nearly as pronounced as at Anza (Fig. 8).

A small sample of data from GRF shows similar behavior. Azimuthal deviations of both particle motion and slowness azimuths are less than 5° , there is very little frequency dependence in the narrowband slowness results, and particle-motion azimuths agree with slowness. The deviations are negative for two western events and positive for an eastern backazimuth (Fig. 9).

Discussion and Numerical Modeling

Nothing in the results from GRF and NORSAR runs counter to expectations. The particle motion and slowness azimuthal deviations at GRF are consistent, relatively small, and frequency independent. The same azimuthal pattern as seen here has been observed in previous studies, and explained by either velocity structure in the crust and upper mantle (Faber *et al.*, 1986) or a sedimentary wedge underneath the array (Krüger and Weber, 1992). It is noteworthy that similar azimuthal behavior is seen in short-period

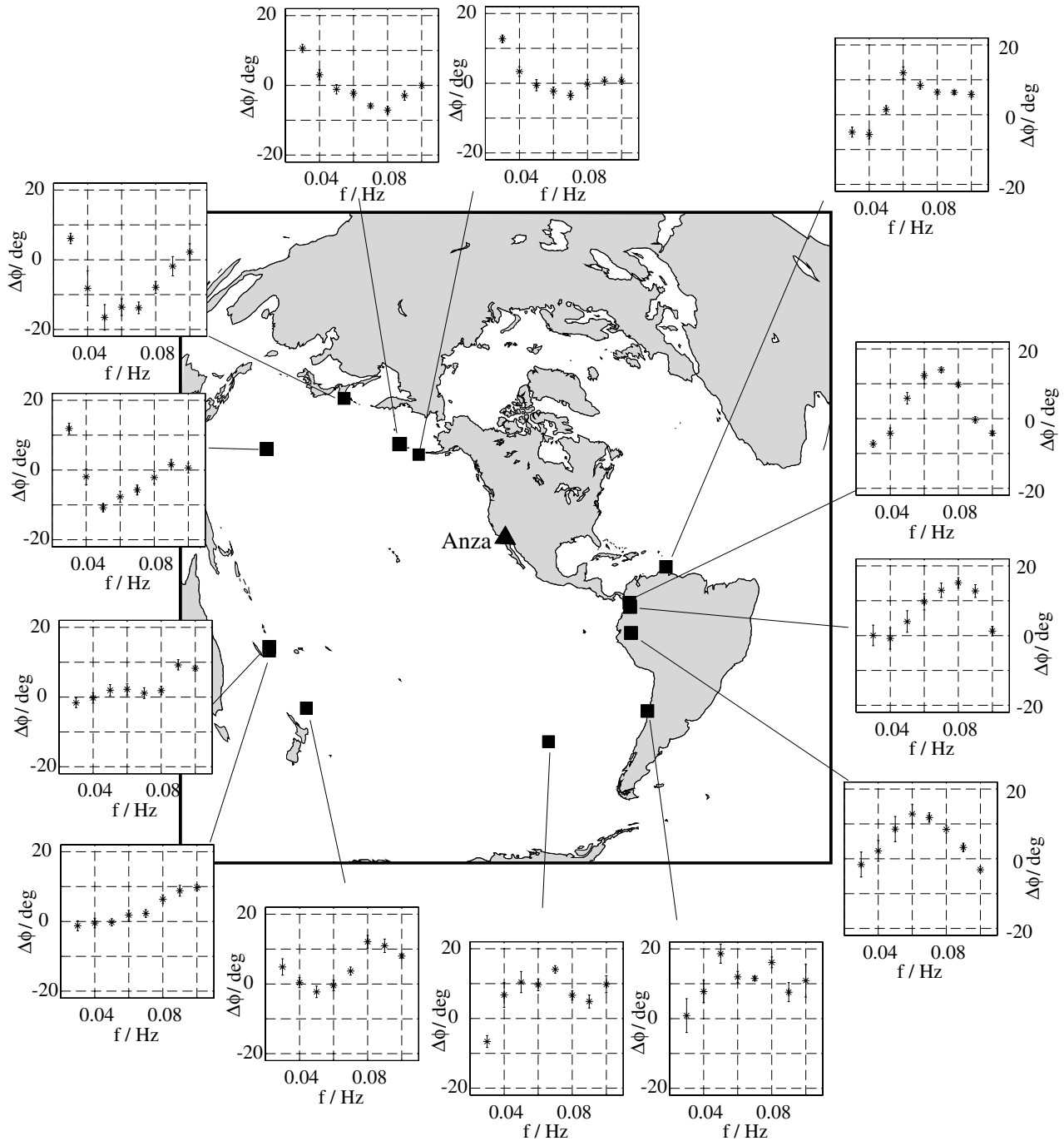


Figure 6. Azimuthal deviation of the slowness vector as a function of frequency for each event, with event and array locations indicated on the map. The projection conserves great circles through the array in the center as straight lines.

(Krüger and Weber, 1992), broad-band (Krüger, 1994), and long-period (this study) data.

Observations at NORSAR are equally uncomplicated; Berteussen (1976) obtained similar results to this study in both short- and long-period bands, and concluded that the anomalies are consistent with structure at depths of less than 100 km underneath the array.

Anza, however, presents a more complicated picture.

The anomalies have much larger amplitudes, show a discrepancy between particle motion and slowness, and are strongly frequency dependent. Although the influence of a sedimentary layer can be excluded for Anza because of its situation on bedrock, the tectonic setting is more complex than that of GRF and NORSAR, neither of which are situated in regions of active tectonics. The shallow crustal *P* velocity structure underneath Anza was found by Scott *et al.* (1994)

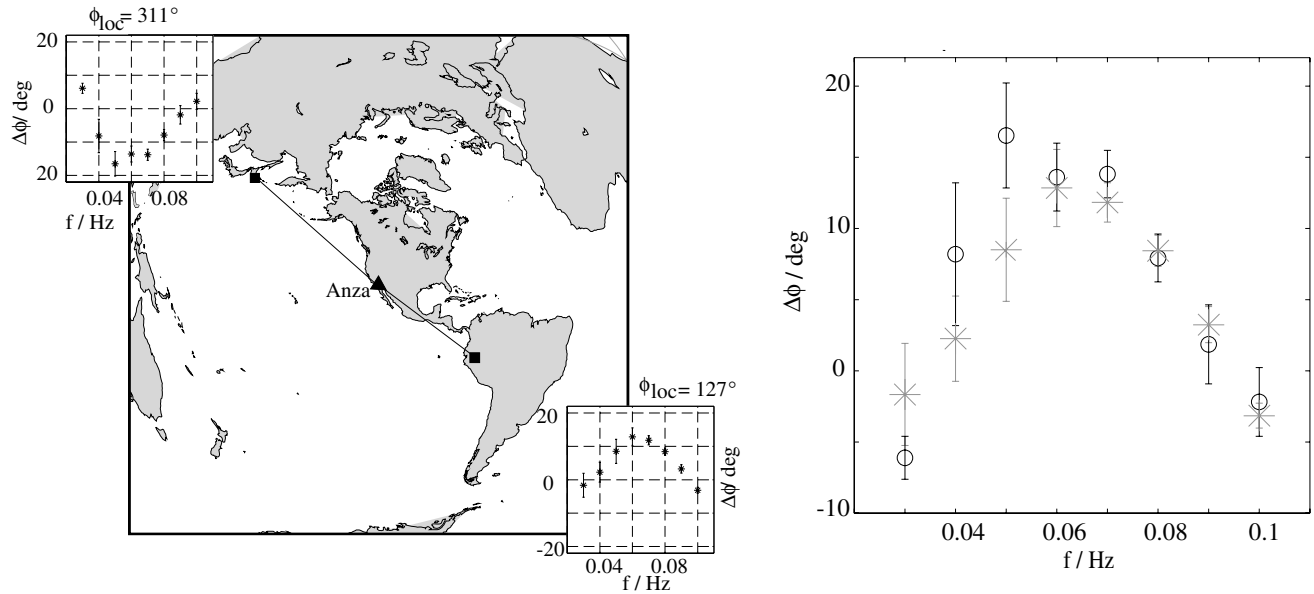


Figure 7. (left) Two events from Figure 6 at opposite backazimuths. (right) Overlay of the anomaly pattern of the event in the NW with reversed sign on the pattern of the SW event.

to be correlated to the San Jacinto fault, which bisects the array from northwest to southeast, with lower velocities south of the fault and up to 20% (~ 1 km/sec) higher velocities on the northern side down to their maximum study depth of 9 km. This would cause negative azimuthal anomalies in slowness for South American events and positive deviations for events in the northwest, which is the opposite of what we observe in the middle frequency range of the long-period band.

Moho topography across Anza has been studied by Lewis *et al.* (2000), who inferred a dip down toward the southwest from receiver functions. Again, this would result in a sense of slowness anomalies opposite to our results. There is some evidence that the upper mantle has the opposite velocity signature, slow underneath the Salton Trough and fast closer to the coast (e.g., from the tomographic studies by Humphreys and Clayton [1990]; Kohler *et al.* (2002); Tanimoto and Prindle-Sheldrake (2002). Similar indications exist for the lower crust (Hauksson, 2000; Hu *et al.*, 1994). Both would serve to explain our observations in the middle-period range qualitatively. Additionally, it seems appropriate to speculate that the complicated slowness behavior with frequency that we observe is due to these contradictory influences at different depths. We tested this hypothesis using a finite difference code that handles 3D isotropic models (Olsen, 1994).

The goal of our forward modeling experiment was to produce slowness azimuthal anomalies and frequency dependence of comparable magnitude to our observations at Anza with realistic velocity perturbations in the crust and upper mantle. The numerical method is a staggered grid finite difference scheme with 4th order accuracy in space and

second order accuracy in time, implemented in a cartesian system containing a cube of $500 \times 500 \times 400$ (depth) km of upper mantle and crust, with a free surface and absorbing boundaries on the sides and bottom. A propagating plane P wave is launched at 200 km depth with an incidence angle of 30° to the vertical. A vertical plane in the middle of the model parallel to the azimuth of incidence separates fast and slow portions of heterogeneous layers. An example of the model geometry is shown in Figure 10. If, for instance, the San Jacinto fault separates fast velocities in the shallow crust on the northeastern side of the array and a slow anomaly on the southwestern side as suggested by Scott *et al.* (1994), this corresponds to modeling an event with a backazimuth parallel to the fault, for example, from South America. Because the observed slowness azimuthal anomalies at Anza appear predominantly antisymmetric about a northwest–southeast axis, we limit the model space to such 2.5D structures with the same symmetry axis. Existing crust and mantle models from tomography suggest a similar northwest–southeast line of separation between fast and slow anomalies (Hauksson, 2000; Kohler *et al.*, 2002; Tanimoto and Prindle-Sheldrake, 2002) and the Moho dip inferred from receiver functions has the same strike as well (Lewis *et al.*, 2000; Zhu and Kanamori, 2000).

The initial model consists of a homogeneous crust atop a homogeneous mantle, both with constant velocities rather than gradients. When adding a layer at the surface with faster velocities on one half and slower velocities on the other half of the model block, the wavefront is sped up on one side and delayed on the other, which results in a change of apparent backazimuth. The azimuthal deviation scales with the strength of the perturbation and the layer thickness. A thin

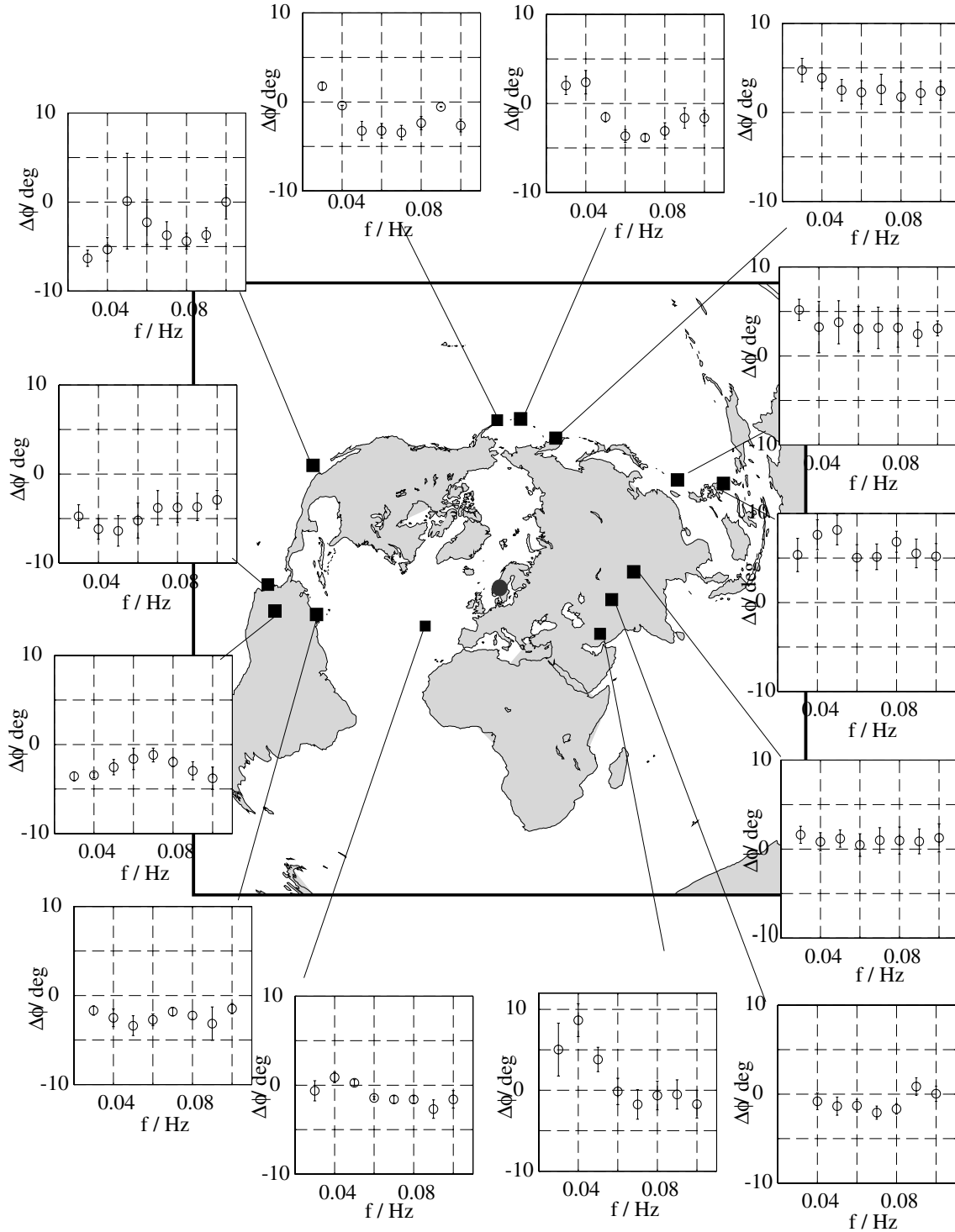


Figure 8. Same as Figure 6, here for NORSAR; note a different scale for $\Delta\phi$.

surface layer affects higher frequencies more strongly than lower frequencies. Similar behavior occurs for an offset in Moho depth along a line perpendicular to the wavefront, which is equivalent to a buried layer with a velocity contrast. For a buried layer, the depth of burial in addition to the perturbation layer thickness affects the frequency depen-

dence. Moho offsets of 5–10 km cause azimuthal deviations of 5° to 10° in the simplified two-layer (homogeneous crust and mantle) models. The frequency dependence of the azimuthal deviation has the same spread of 5° to 10° in these cases.

An anomalous layer in the mantle with 4% fast and slow

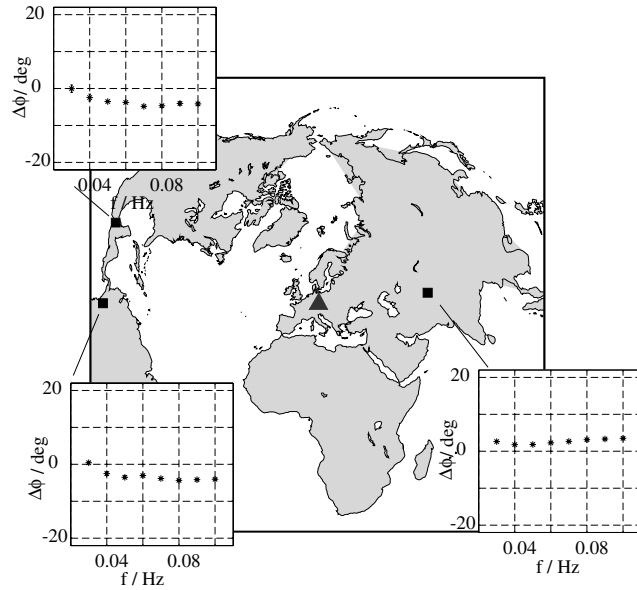


Figure 9. Same as Figure 6, here for GRF.

velocity perturbations on opposite sides of the model causes azimuthal deviations of 15° to 25° , with the larger deviations for thicker anomalous layers that lie closer to the surface. Depending on the depth of the anomalous layer, the size of the deviation as a function of frequency is either monotonic, with the maximum values at long periods (Fig. 10), or shows a minimum at intermediate periods. This is contrary to our observations for events incident along the southeast–northwest azimuth, which show maximum deviations at intermediate periods. The latter effect can be achieved with two rather than one heterogeneous layer with opposing signs of the anomaly, similar to the situation suggested by the tomographic studies. One candidate model that causes a variation in the azimuthal wavefront deviation over frequency of 10° with a maximum at intermediate frequencies has a 5% velocity anomaly in the lower half of the crust and a 4% anomaly in a 25-km mantle layer below the Moho (Fig. 11). The sign of these velocity anomalies is suggested in the models of Hauksson (2000) for the lower crust (fast southwest of San Jacinto fault, slow northeast) and Kohler *et al.* (2002) for the uppermost mantle (slow southwest, fast northeast), although the velocity perturbations there are smaller by a factor of 2 and 4. Because of the sensitivity of the frequency-dependent behavior to layer thicknesses, this forward modeling approach is highly nonunique. A slight change of the

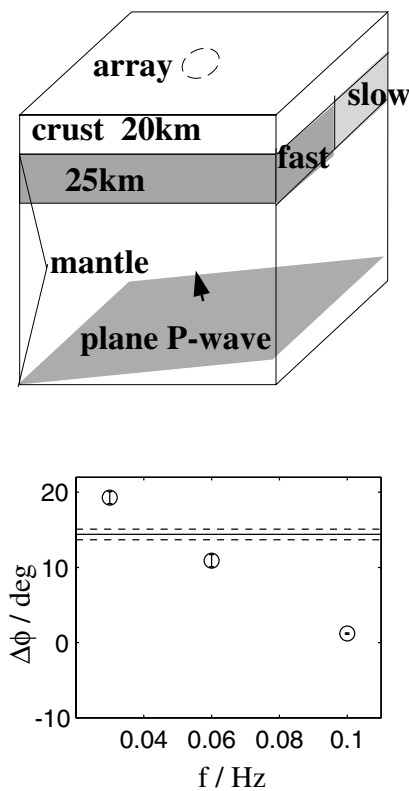


Figure 10. (top) Geometry for 3D finite difference modeling. The background P velocity is 6.3 km/sec in the crust and 8.1 km/sec in the mantle. The perturbation layer at the top of the mantle has 4% fast and slow anomalies in each half of the model. (bottom) Azimuthal slowness perturbation for the model in the top panel as a function of frequency (circles with error bars) and for the unfiltered synthetic (solid line, error dashed lines).

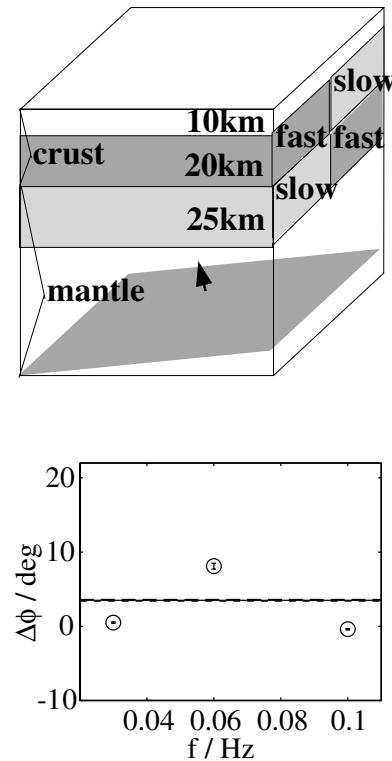


Figure 11. (top) Background velocities same as in Figure 10. The perturbation is 5% in the crust and 4% in the mantle. (bottom) Azimuthal slowness perturbation for the model in the top panel as a function of frequency, legend as in Figure 10.

layer thicknesses and perturbation strength can result in significantly different slowness azimuths (Fig. 12). An addition of anisotropy and gradients in the model layers or 3D rather than 2.5D structure would make the fit to our observations even less well determined. Anisotropy in horizontally layered structures will not affect slowness; however, in 2D structures such as those modeled here, there will be a trade-off between effects of anisotropy and heterogeneity. Rather than trying to fit our slowness observations exactly, we have demonstrated that it is possible to produce the observed azimuthal deviations with realistic isotropic crust and mantle velocity perturbations. An attempt to find a well-constrained model that fits our data exactly will require additional constraints as well as modeling with an anisotropic 3D code.

Conclusions

We analyzed slowness and particle-motion azimuthal anomalies of long-period teleseismic *P* at three broadband arrays. The two arrays in tectonically stable regions, NORSAR on the Scandinavian shield in southern Norway and GRF in the Frankenjura in southeastern Germany, show consistent behavior between slownesses and particle mo-

tions, with small azimuthal deviations on the order of 5° and little to no frequency dependence in the long-period band. The observations are similar to those of previous studies which inferred structure in the crust and uppermost mantle to explain their results.

In contrast, data from the Anza array situated in an area with active tectonics show azimuthal anomalies in both particle motion and slowness on the order of $\sim 20^\circ$, with up to a 20° difference between the two observables. In addition, there is a strong frequency dependence of the slowness azimuth within the long-period band. We postulate that the discrepancy between particle motion and slowness is due to anisotropy, whereas the frequency dependence of the slowness azimuths is caused by velocity anomalies of opposing signs with depth suggested in the literature. The latter is supported by numerical modeling experiments with a 3D finite difference code.

Acknowledgments

GRF and Norsar data were made available by the Seismological Central Observatory (SZGRF) and NORSAR, respectively. Kim Olsen provided a copy of his 3D finite difference code and added a plane wave source routine. We would also like to thank Guy Masters, Peter Shearer, Donna Blackman, and Gary Pavlis for helpful discussions, and Ileana Tibuleac, Lee Steck, and Anton Dainty for reviews of the manuscript. This work was supported by National Science Foundation Grant EAR-9902422.

References

- Berteussen, K. A. (1976). The origin of slowness and azimuth anomalies at large arrays, *Bull. Seism. Soc. Am.* **66**, 719–741.
- Chiou, S., and B. A. Bolt (1993). Seismic wave slowness-vector estimation from broad-band array data, *Geophys. J. Int.* **114**, 234–248.
- Crampin, S., R. A. Stephen, and R. McGonigle, The polarization of *P*-waves in anisotropic media, *Geophys. J. R. Astr. Soc.* **68**, 477–485.
- Faber, S., J. Plomerova, and V. Babuska (1986). Deep seated lateral velocity variations beneath the GRF array inferred from mislocation patterns and *P* residuals, *J. Geophys.* **60**, 139–148.
- Harris, D. B. (1990). Comparison of the direction estimation performance of high-frequency seismic arrays and three-component stations, *Bull. Seism. Soc. Am.* **80**, 1951–1968.
- Hauksson, E. (2000). Crustal structure and seismicity distribution adjacent to the Pacific and North America plate boundary in southern California, *J. Geophys. Res.* **105**, 13,875–13,903.
- Hu, G., W. Menke, and C. Powell (1994). Polarization tomography for *P* wave velocity structure in southern California, *J. Geophys. Res.* **99**, 15,245–15,256.
- Humphreys, E. D., and R. W. Clayton (1990). Tomographic image of the southern California mantle, *J. Geophys. Res.* **95**, 19,725–19,746.
- Kohler, M. D., H. Magistrale, and R. W. Clayton (2003). Mantle heterogeneities and the SCEC Reference Three-Dimensional Seismic Velocity Model Version 3, *Bull. Seism. Soc. Am.* **93**, no. 2, 757–774.
- Krüger, F. (1994). Sediment structure at GRF from polarization analysis of *P* waves of nuclear explosions, *Bull. Seism. Soc. Am.* **84**, 149–170.
- Krüger, F., and M. Weber (1992). The effect of low-velocity sediments on the mislocation vectors of the GRF array, *Geophys. J. Int.* **108**, 387–393.
- Lewis, J., S. M. Day, H. Magistrale, J. Eakins, and F. Vernon (2000). Regional crustal thickness variations of the peninsular ranges, southern California, *Geology*, **28**, 303–306.
- Lin, C.-H., and S. W. Roecker (1996). *P*-wave backazimuth anomalies

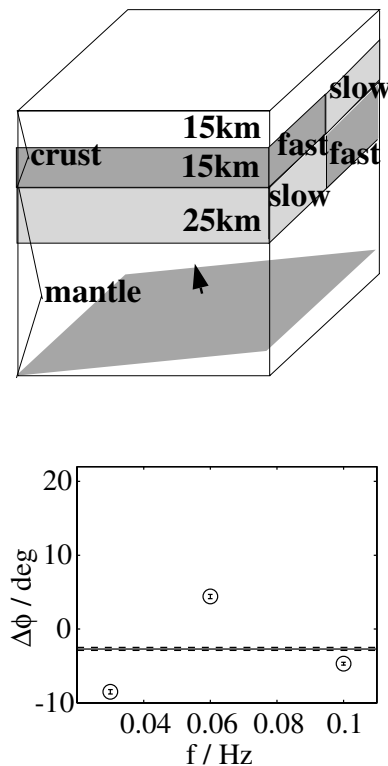


Figure 12. (top) A slight change in layer thickness and perturbation strength from the model in Figure 11. Background velocities same as in Figure 10. The perturbation is 4% in crust and mantle. (bottom) Azimuthal slowness perturbation for the model in the top panel as a function of frequency, legend as in Figure 10.

- observed by a small-aperture seismic array at Piñon Flat, California: implications for structure and source location, *Bull. Seism. Soc. Am.* **86**, 470–476.
- Olsen, K. B. (1994). Simulation of three-dimensional wave propagation in the Salt Lake Basin, *Ph.D. thesis*. University of Utah, Salt Lake City, Utah.
- Schulte-Pelkum, V., G. Masters, and P. M. Shearer (2001). Upper mantle anisotropy from long-period *P* polarization, *J. Geophys. Res.*, **106**, 21,917–21,934.
- Scott, J. S., T. G. Masters, and F. L. Vernon (1994). 3-D velocity structure of the San Jacinto fault zone near Anza, California; i, *P* waves, *Geophys. J. Int.* **119**, 611–626.
- Steck, L., and W. A. Prothero (1993). Observations of direct *P*-wave slowness and azimuth anomalies for teleseisms recorded in Long Valley Caldera, California, *Bull. Seism. Soc. Am.* **83**, 1391–1419.
- Tanimoto, T., and K. Prindle-Sheldrake (2002). Three-dimensional S-wave velocity structure in Southern California, *Geophys. Res. Lett.* **29**, no. 8, 10.1029/2001GL013486.
- Tibuleac, I., and E. Herrin (1999). Lower mantle lateral heterogeneity beneath the Caribbean Sea, *Science* **285**, 1711–1715.
- Wagner, G. S., and T. J. Owens (1996). Signal detection using multi-channel seismic data, *Bull. Seism. Soc. Am.* **86**, 221–231.
- Zhu, L., and H. Kanamori (2000). Moho depth variation in southern California from teleseismic receiver functions, *J. Geophys. Res.*, **105**, 2969–2980.

Institute of Geophysics and Planetary Physics
 Scripps Institution of Oceanography
 University of California, San Diego
 La Jolla, California 92093-0225
 vschulte@ucsd.edu

Manuscript received 23 May 2002.